Production and Mass-Spectroscopic Characterization of Multiple Metal-Rich Alkali Halide Ion Clusters: Novel Structures and Properties

Toshiki Sugai and Hisanori Shinohara*

Department of Chemistry, Nagoya University, Nagoya 464-8602

(Received July 26, 1999)

Multiple metal-rich ion alkali halide clusters from solid crystals of NaF and CsI have been produced and characterized for the first time by a newly developed high-pressure laser-vaporization cluster source. The observed positive metal-rich clusters are $Na_nF_m^+$ ($n \approx 40$, $n-m = 1$—9) and $Cs_nI_m^+$ ($n \approx 60$, $n-m = 0$—5), which have enhanced intensities at $n = 14$, being independent of m, indicating the existence of multiple excess electrons. For negative clusters, $Na_nF_m^-$ ($n \approx 40$, $n-m = -1$—10) and $Cs_nI_m^-$ ($n \approx 60$, $n-m = -2$—3) have been observed. The NaF metal-rich negative clusters show two types of distinct magic numbers at $n-m = 7$ ($(NaF)_mNa_7^-$) and $n = 14$ ($Na_{14}F_{13-x}^-$, $x = 0$—4). The former and latter magic-number ions suggest the existence of a negative core ion of Na_7^- and a cubic $3\times3\times3$ structure with multiple excess electrons, respectively. The present high-pressure laser-vaporization cluster source is suitable to produce these unstable clusters with a unique stoichiometry.

The structures, electronic properties and size effects of alkali halide (AX) clusters have been studied for the last decade.[1—9] AX clusters have been produced so far by using such methods as an oven,[1,2] laser vaporization,[5,8,9] fast-atom bombardment,[3] and the reaction method[2,4,6,7] where metal vapor reacts with halogen-containing seed gases. The AX clusters produced by these methods, except for the reaction method,[2,4,6,7] have provided known stoichiometrical species, $Na^+(NaCl)_n$ and $Cl^-(NaCl)_n$, in which the ionic interaction dominates, even in small clusters ($n \approx 4$). The positive and negative charges are localized at metal cations and halogen anions in the clusters, respectively.[10—13] From the observed magic-number features,[14—16] these clusters have been thought to exhibit a rock-salt structure and is normally observed in the bulk state, which is supported by several theoretical studies.[1—3] Recent studies by two-photon ionization spectroscopy[6,7] and ion mobility measurements[8,9] on the structure of AX clusters have shown, however, the presence of novel states, such as a color center, trapped electrons on the surface defects, delocalized electrons on the surface, surface vacancies, and loosely attached metal atoms. These novel structures of AX clusters are strongly dependent on those defects incorporated with excess metal atoms.

Metal-rich alkali halide (MR-AX) clusters, such as $Na_{14}F_{12}^+$ with one excess metal atom, in reference to the normal type $(Metal)_n(Halide)_m^+$ ($n-m = 1$), have been produced only by the reaction method.[2,4,6,7] Multiple MR-AX clusters, $(Metal)_n(Halide)_m^+$ ($n-m \geq 2$), on the other hand, have not been produced by the normal laser-vaporization method. Theoretical calculations suggest that MR-AX clusters with one excess metal atom have F-center like structures with an excess electron, and that a magic number appears at $n = 14$ with an assumed $3\times3\times3$ cubic structure.[17—20] Landman and co-workers have shown that multiple MR-AX clusters ($n-m \geq 3$) have multiple vacancies and that the excess electrons are trapped at the vacancies so as to maintain some stable cubic structures.[18] They also reported that the presence of further excess metal atoms leads to phase separation between metal clusters and AX clusters.[18] Experimentally, Whetten and coworkers have reported that an MR-AX cluster of $Na_{14}F_{12}^+$ with one excess metal atom has a $3\times3\times3$ cubic structure.[4,17,21] Poncharal and coworkers have produced neutral multiple MR-AX clusters by reaction methods.[6] Despite these efforts, production and structural studies of MR-AX ion clusters with multiple excess metal atoms ($n-m \geq 3$) have not yet been achieved because of their structural and electronic instability. Here, we report the first successful production of MR-AX positive and negative clusters with multiple excess electrons. The results also indicate that the negative MR-AX clusters separated into a metal ion cluster and an AX cluster.[11,22]

Experimental

The details of the cluster beam source have been described elsewhere.[10—13,22] Briefly, the source consists of a preload pulsed valve, a main pulsed valve, an evaporation room with an X stage and holes for a laser and a cluster beam, and a rectangular sample plate mounted on a Y–Z stage (Fig. 1). A sample (NaF or CsI) was periodically translated in a zigzag motion by the Y–Z stage so that laser vaporization could occur in a fresh surface of the sample plate. A General Valve (Model 9-279-900) and a Jordan Valve (PSV Pulsed Supersonic Molecular Valve) were used as the preload valve and the main valve, respectively. A cooling (buffer) gas, typically He, was introduced into the evaporation room (1—10 Torr, 1 Torr = 133.322 Pa) from the preload valve. This achieved a quasi-

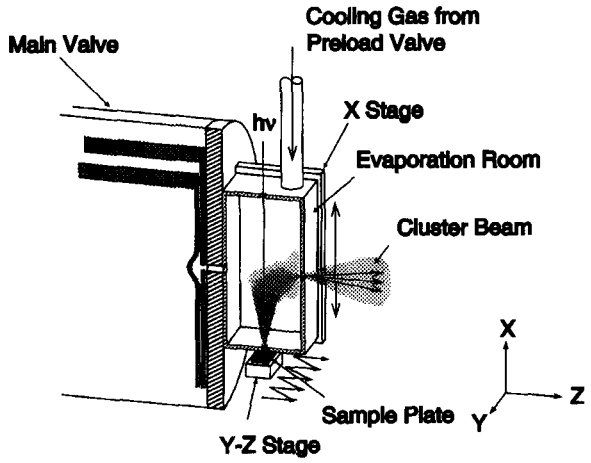

Fig. 1. A schematic diagram of a high-pressure laser-vaporization cluster beam source.

fluxless condition, which was suitable for the production of large and annealed clusters as well as ultrafine particles.[23] After a suitable delay (ca. 700 μs from the cooling gas injection), a 532 nm light pulse from a YAG laser was introduced, which vaporized the sample surface. The produced clusters grew and were annealed in the cooling gas. The clusters were then ejected into a reflectron TOF mass spectrometer by supersonic jets of He (10 atm) from the main pulsed valve.

To optimize the production of MR-AX clusters, the temperature of the evaporation room was varied between 160 and 298 K. The residence time of the cooling gas in the evaporation room was estimated to be 300—1000 μs, where thermal equilibrium could be achieved.

Results

Figure 2 shows the mass spectra of positive cluster ions of NaF and CsI. The observed NaF and CsI clusters are $Na_nF_m^+$ ($n-m$ = 1—9, $n \approx 40$) at 190 K and $Cs_nI_m^+$ ($n-m$ = 0—5, $n \approx 60$) at 180 K, respectively. The mass spectra show the well-known magic-number peaks at $(n, m) = (5,4)$, (14, 13), and (23, 22). Figures 2(a) and 2(b) show the presence of metal-rich clusters adjacent to the conventional alkali halide clusters. The intensity of the MR-AX clusters decreases as the metalization sequence increases, whereas it becomes more prominent as the temperature of the evaporation room decreases (298—160 K). These results suggest that the MR-AX clusters are less stable compared with the conventional clusters. MR-AX clusters have so far been produced only by gas-phase reactions where the observed maximum number of excess metal atoms was two.[2,4,17] The present high-pressure gas-evaporation cluster source can produce clusters with a high degree of metalization and clustering.

Figures 3 and 4 show the intensity distribution of MR-AX clusters of $Na_nF_m^+$ and $Cs_nI_m^+$, respectively. The mass spectra were obtained by averaging 1×10^3—3×10^3 shots. The average number of ions at one peak was estimated to be 10^2—10^4. If the ion intensity follows a Poisson distribution, that is, there is no special condition change during the experiment, the standard deviation of the intensity distribution is less than 1%.[24] The deviation (σ) is estimated from the

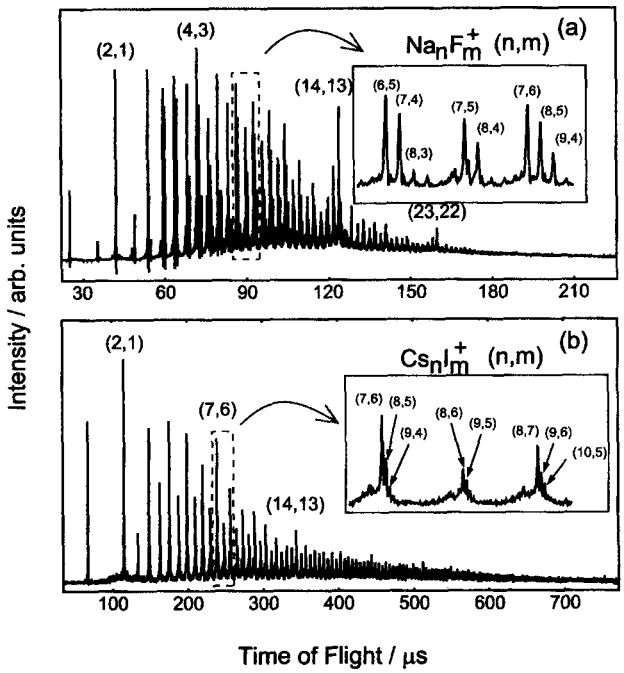

Fig. 2. (a), (b): Mass spectra of positive metal-rich alkali halide clusters of Na_nF_m, ($n-m$ = 1—4) at 170 K, and Cs_nI_m, ($n-m$ = 0—5) at 160 K, respectively.

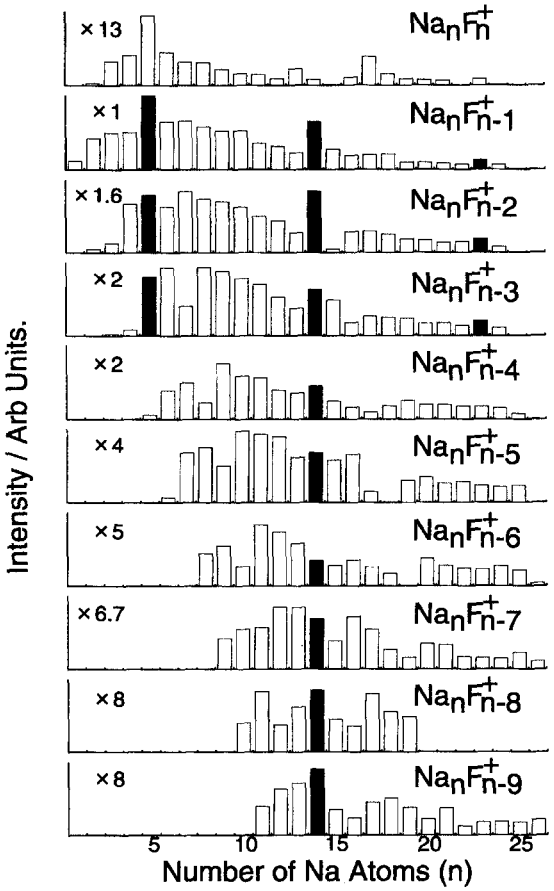

Fig. 3. Intensity distribution of NaF metal-rich positive ion clusters on the number of Na atoms.

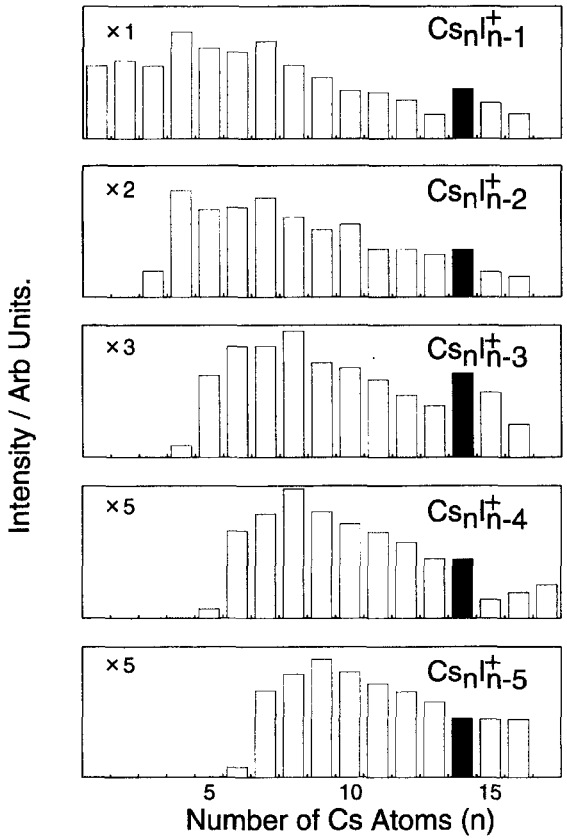

Fig. 4. Intensity distribution of CsI metal-rich positive ion clusters on the number of Cs atoms.

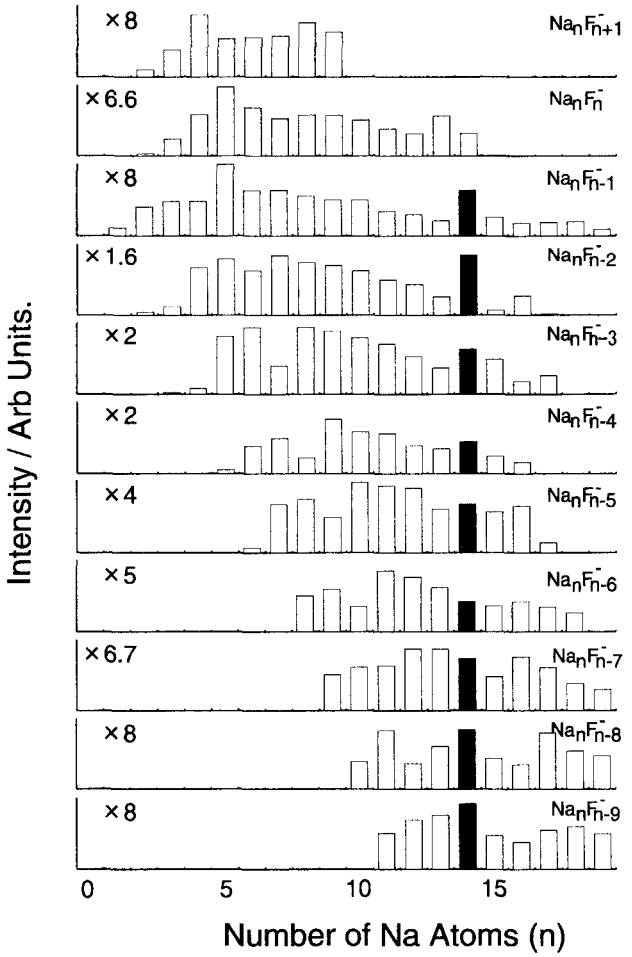

Fig. 5. Intensity distribution of NaF metal-rich negative ion clusters with stoichiometry of $Na_nF_{n-m}^-$ ($m = -1$—9) on the number of Na atoms produced in a NaF-rich Na-poor condition.

average number of ions (C) and the number of shots (N) as $\sigma = \sqrt{C/N}$. The base-line noise levels of the spectra are also within this deviation. The intensities of each species were obtained from the area of the mass peaks. Most of the positive MR-AX clusters shows enhanced peaks at $n = 14$ (filled squares), some of which (such as $Na_{14}F_{12}^+$) can be regarded as magic numbers. Figure 3 shows less enhanced peaks at $n = 5$ and 23.

Negative MR-AX clusters of $Na_nF_m^-$ and $Cs_nI_m^-$ were also produced by using the source with more excess metal atoms (ca. 15) than those of positive MR-AX clusters (ca. 9). Figures 5 and 6 show that the intensity distribution of $Na_nF_m^-$ is strongly dependent on the production condition. Figure 5 shows the same magic features at $n = 14$ as those of positive MR-AX clusters (Fig. 3) in a NaF-rich and Na-poor condition, whereas Fig. 6 does not show any magic features at $n = 14$. The production condition of Fig. 6 is a Na-rich and NaF-poor condition.

The NaF-rich and Na-poor condition is realized by using higher laser power and a higher buffer gas temperature (around 250 K). The Na-rich and NaF-poor condition is obtained in a lower laser power and a lower buffer gas temperature (below 200 K).

Figure 7 shows the intensity distribution of NaF negative MR-AX clusters of Fig. 6 with a different stoichiometrical notation of $(NaF)_mNa_n^-$ on the number of excess metal atoms (n) produced under the same condition as in Fig. 6. The result shows that magic numbers appear at $n = 7$ ($3 \leq m \leq 7$), which shows the existence of stable Na_7^- clusters in the negative MR-AX clusters. However, the magic numbers at $n = 7$ disappear when a part of the AX cluster in the negative MR-AX clusters become larger ($m \geq 8$). Under both conditions, no large pure metal clusters, like Na_7^-, are produced. Negative CsI MR-AX clusters do not show any distinct magic features on the number of excess metal atoms.

Discussion

The magic-number features at $n = 14$ of positive multiple MR-AX clusters (Figs. 3 and 4) are the same as those of the normal AX clusters, which suggest that the normal AX clusters have the cubic $3\times3\times3$ structure. The present results reveal that the MR-AX clusters also have the stable cubic $3\times3\times3$ structure.[22] The other magic features at $n = 5$ and $n = 23$ can be interpreted as indicating the presence of F-center cubic structures with $3\times3\times1$ for $n = 5$ and $3\times3\times5$ for $n = 23$, which is consistent with formation of F-center type clusters with multiple excess electrons. At lower temperatures, clusters can attain an enhanced stabilization to form MR-AX clusters.

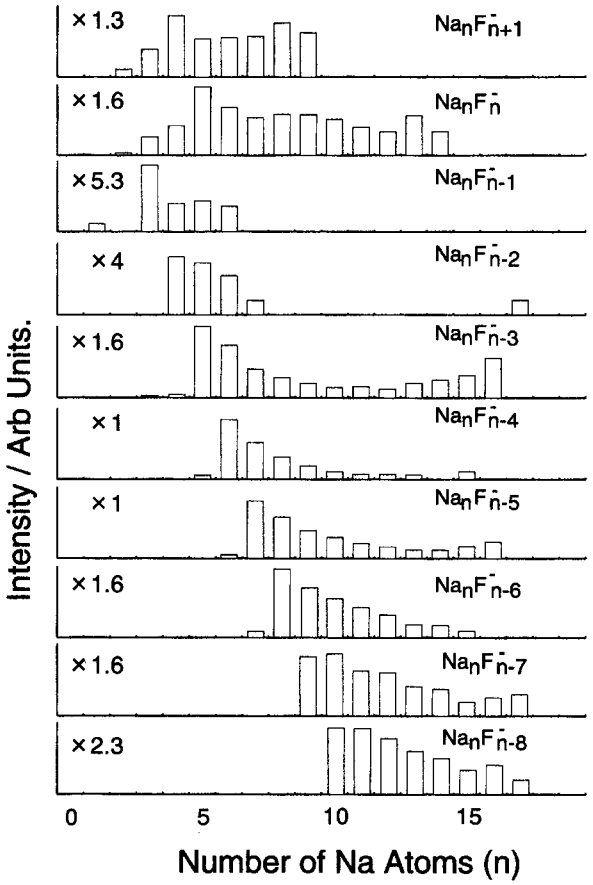

Fig. 6. Intensity distribution of NaF metal-rich negative ion clusters with stoichiometry of $Na_nF_{n-m}^-$ ($m = -1$—16) on the number of Na atoms produced in a Na-rich and NaF-poor condition.

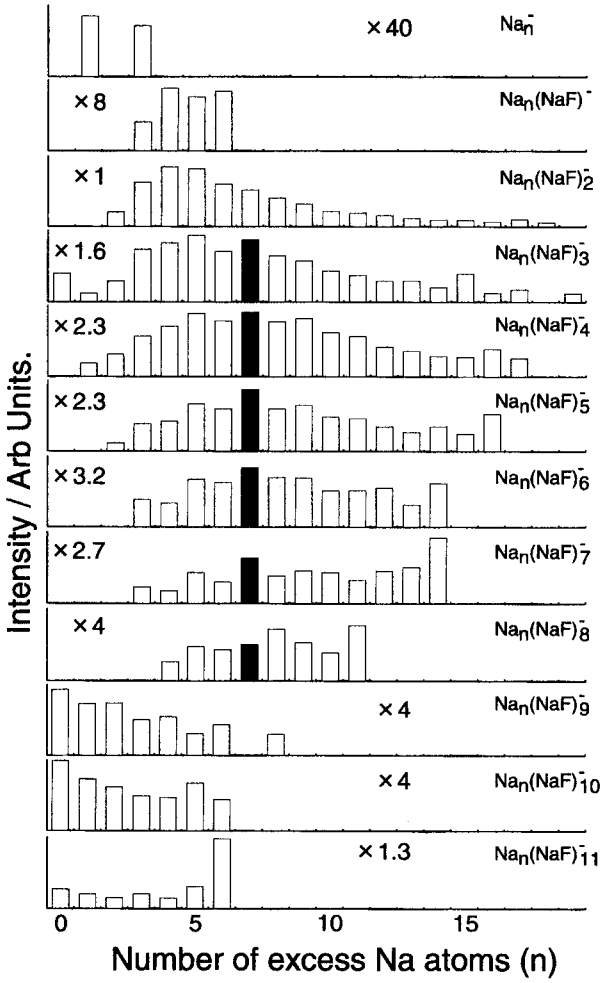

Fig. 7. Intensity distribution of NaF metal-rich negative ion clusters with stoichiometry of $Na_n(NaF)_m^-$ ($m = 0$—11) on the number of excess Na atoms produced in a Na-rich and NaF-poor condition.

These structures seem to stem not only from energetical stability, but also from growth processes of those clusters. Figures 3 and 4 show that the MR-AX clusters appear from $(Na_2F)^+Na_{n'}$ and $(Cs_2I)^+Cs_{n'}$ or $(Na_3F_2)^+Na_{n'}$ and $(Cs_3I_2)^+Cs_{n'}$. These results imply that the onset clusters are produced by aggregation between the "core" positive clusters, such as $(Na_2F)^+$ or $(Na_3F_2)^+$, and neutral alkali metal atoms or alkali halide molecules. These "core" clusters are conventional AX clusters, which were reported to be produced by fragmentation processes.[27] Therefore, the intensity distributions of these MR-AX clusters depend on the stability of the "core" clusters. For example, Fig. 4 shows that the most abundant species have the stoichiometry of $(Cs_5I_4)^+Cs_{n'}$ or $(Cs_4I_3)^+Cs_{n'}$, indicating the presence of the stable $(Cs_5I_4)^+$ and $(Cs_4I_3)^+$ core ions. These production models can explain that medium metalization clusters show less enhanced peaks at $n = 14$, such as $Na_{14}F_{14-m}^+$ ($m = 5$—7) or $Cs_{14}I_{14-m}^+$ ($m = 5$). In these cases, the "core" clusters are $Cs_{10}I_9^+$ or $Na_8F_7^+$. These "core" clusters may have different properties from larger or smaller "core" clusters, such as $Na_{13}F_{12}^+$ or $Na_5F_4^+$, which eventually become the cubic MR-AX clusters.

The negative NaF MR-AX clusters, on the other hand, have two types of magic features, depending on the production conditions: $Na_nF_m^-$ at $n = 14$ in Fig. 5 and $(NaF)_mNa_n^-$ at $n = 7$ in Fig. 7. When the NaF negative MR-AX clusters are produced under the NaF-rich and Na-poor condition (Fig. 5), the magic-number species appear at $Na_{14}F_{13-x}$ ($x = 0$—8). This stoichiometry is the same as that of the positive MR-AX clusters, and the presumed structures are the cubic $3\times3\times3$. Under the NaF-poor and Na-rich condition (Fig. 7), the negative NaF MR-AX clusters show the magic-number features at $(NaF)_mNa_n^-$ ($n = 7$). These magic-number features suggest the presence of a Na_7^- ion core in the clusters. Theoretical[25] and experimental[26] studies have shown that the Na_7^- cluster is electronically stable because of the closed electronic shell structure. The results indicate that these NaF negative MR-AX clusters produced under the Na-rich and NaF-poor condition are separated into metal clusters and normal AX clusters.

The disappearance of the magic-numbers features of MR-AX clusters having larger AX cluster components ($(NaF)_mNa_n^-$, $m \geq 9$) suggests the presence of two distinct cluster structures. The clusters with $m \geq 9$ form $(NaF)_m$ ion cores with individual Na atoms attached to the cluster sur-

face. Below m = 9, Na metal clusters are formed segregated from the $(NaF)_m$ ion cores. These structures and the production mechanisms are consistent with the absence of large pure metal negative clusters (Figs. 5, 6, and 7). The MR-AX clusters are not produced from the pure metal clusters and AX molecules but from negative AX clusters and neutral metal atoms. The negative AX clusters attract neutral metal atoms on the surface and the MR-AX clusters are produced.

Such a variety of the structures of the negative ion MR-AX clusters stem from the smaller binding energies of these clusters compared to those of positive MR-AX clusters. The two types of clusters may have almost the same stability and transform easily into each other. The negative CsI MR-AX clusters do not show any magic features like those of the negative NaF MR-AX clusters. This can be interpreted by the smaller ionic properties of the CsI negative MR-AX clusters than those of the NaF negative MR-AX clusters and the CsI positive MR-AX clusters.

The present work has been supported by Grants-in-Aid for Scientific Research (A) (2) (No. 08554020) and Scientific Research (B) (2) (No. 09440198) from the Ministry of Education, Science, Sports and Culture.

References

1 R. Pflaum, P. Pfau, K. Sattler, and E. Recknagel, *Surf. Sci.*, **156**, 165 (1985).

2 T. P. Martin, *Surf. Sci.*, **156**, 584 (1985).

3 I. Katakuse, T. Ichihara, H. Ito, T. Matsuo, T. Sakurai, and H. Matsuda, *Rapid Comm. Mass Spectrom.*, **2**, 191 (1988).

4 E. C. Honea, M. L. Homer, P. Labastie, and R. L. Whetten, *Phys. Rev. Lett.*, **63**, 394 (1989).

5 Y. J. Twu, C. W. S. Conover, Y. A. Yang, and L. A. Bloomfield, *Phys. Rev. B*, **42**, 5306 (1990).

6 P. Labastie, J.-M. L'Hermite, P. Poncharal, and M. Sence, *J. Chem. Phys.*, **103**, 6362 (1995).

7 G. Durand, F. Spiegelmann, P. Labastie, J.-M. L'Hermite, and P. Poncharal, *Phys. Rev. Lett.*, **79**, 633 (1997).

8 R. R. Hudgins, P. Dugourd, J. M. Tenenbaum, and M. F. Jarrold, *Phys. Rev. Lett.*, **78**, 4213 (1997).

9 P. Dugourd, R. R. Hudgins, and M. F. Jarrold, *Chem. Phys. Lett.*, **267**, 186 (1997).

10 T. Sugai and H. Shinohara, *Chem. Phys. Lett.*, **264**, 327 (1997).

11 T. Sugai and H. Shinohara, *Z. Phys. D*, **40**, 131 (1997).

12 T. Kimura, T. Sugai, H. Shinohara, K. Tohji, and I. Matsuoka, *Chem. Phys. Lett.*, **246**, 571 (1995).

13 T. Kimura, T. Sugai, and H. Shinohara, *Chem. Phys. Lett.*, **256**, 269 (1996).

14 N. G. Phillips, C. W. S. Conover, and L. A. Bloomfield, *J. Chem. Phys.*, **94**, 4980 (1991).

15 P. Weis, C. Ochsenfeld, R. Ahlrichs, and M. M. Kappes, *J. Chem. Phys.*, **97**, 2553 (1992).

16 C. Ochsenfeld and R. Ahlrichs, *J. Chem. Phys.*, **97**, 3487 (1992).

17 G. Rajagopal, R. N. Barnett, A. Nitzan, U. Landman, E. C. Honea, P. Labastie, M. L. Homer, and R. L. Whetten, *Phys. Rev. Lett.*, **64**, 2933 (1990).

18 G. Rajagopal, R. N. Barnett, and U. Landman, *Phys. Rev. Lett.*, **67**, 727 (1991).

19 J. L. Chen, C. S. Wang, K. A. Jackson, and M. R. Pederson, *Phys. Rev. B.*, **45**, 1927 (1992).

20 G. Durand, J. Giraud-Girad, D. Maynau, and F. Spiegelmann, *J. Chem. Phys.*, **110**, 7871 (1999).

21 R. D. Beck, P. S. John, M. L. Homer, and R. L. Whetten, *Chem. Phys. Lett.*, **187**, 122 (1991).

22 T. Sugai and H. Shinohara, *Chem. Phys. Lett.*, **281**, 57 (1997).

23 R. Uyeda, *Prog. Mater. Sci.*, **35**, 1 (1991).

24 W. H. Press, S. A. Teukolsky, W. T. Vetterling, and B. P. Flannery, "Numerial Recipes in C," Cambridge University Press, Cambridge (1992).

25 W. Knight, K. Clemenger, W. A. d. Heer, W. A. Saunders, M. Chou, and M. L. Cohen, *Phys. Rev. Lett.*, **52**, 2141 (1984).

26 W. Knight, W. A. d. Heer, and W. A. Saunders, *Z. Phys. D*, **3**, 109 (1986).

27 Y. A. Yang, P. Xia, A. L. Junkin, and L. A. Bloomfield, *Phys. Rev. Lett.*, **66**, 1205 (1991).